Engineering Structures 101 (2015) 163–178

Contents lists available at ScienceDirect

Engineering Structures

journal homepage: www.elsevier.com/locate/engstruct

Accurate finite element modeling of pretensioned prestressed concrete beams

O. Yapar [a,1], P.K. Basu [b,*], N. Nordendale [c]

[a] Dassault Systèmes Simulia Corp, 1301 Atwood Ave, Suite 101W, Johnston, RI 02919, United States
[b] Department of Civil and Environmental Engineering, Vanderbilt University, 2201 West End Ave, Nashville, TN 37235, United States
[c] The Aerospace Corporation, 2310 E. El Segundo Blvd., El Segundo, CA 90245, United States

ARTICLE INFO

Article history:
Received 19 August 2014
Revised 13 July 2015
Accepted 14 July 2015

Keywords:
Finite element method
Prestressed concrete
Nonlinear analysis
Plastic-damage
Bond-slip

ABSTRACT

This paper presents a nonlinear finite element model for pretensioned prestressed concrete beams. The study presented here is an important step because it is, perhaps, for the first time that a prestressed concrete beam has been successfully modeled by nonlinear finite element analysis, allowing for plasticity and damage behavior of concrete and slip-bond failure behavior for strands. The model faithfully follows the actual loading history realistically, allowing for the construction sequence including the process of transfer of strand force. Existing results of finite element analysis are not reliable in the critical regions. Even the very recent ones do not seem to have been successful. In this study, all material and bond models used are based on experimental data. The simulation results are validated with data from actual load testing. Apart from examining the behavior of the beam up to the limit state, the response of the damaged beam after local bonded composite patch repair is also considered. For this purpose, the prestressed concrete beam specimens are manufactured and tested in the laboratory before and after they have been repaired with bonded composite patches. Satisfactory agreement between finite element predictions and test results of the virgin beam is noted.

1. Introduction

In prestressed concrete structures, flexural tensile resistance capacity is induced by creating initial compressive stresses in concrete using high strength steel tendons. In precast construction, the pre-compression is induced in the concrete due to the shortening tendency of the released strand, by mobilizing the bond resistance between the two. The conventional mechanics based methods to determine the stress distribution in a prestressed concrete beam caused by various external effects is accurate enough for practical design purposes in the elastic range, except perhaps near the end regions. The main objectives of this paper are (i) to accurately predict the behavior of a precast prestressed concrete beam for all loading stages, and (ii) to predict the performance of a damaged beam subjected to bonded composite patch repair, using nonlinear finite element modeling and simulation. The simulation model needs to reflect the true mechanics of a precast prestressed concrete beam for all stages of loading: manufacture, service condition, and limit state. The simulation model should consider nonlinear material properties reflecting concrete plasticity and damage, interfacial bond characteristics between concrete and steel, and that between concrete and bonded composite patch repair, if used. Interfacial slippage, Poisson radial expansion of the strands, and wedging (or, Hoyer) effect at the ends also need to be accounted for. For the purpose of this study, a test prestressed concrete beam is considered. A four-point load test is first undertaken on the prestressed concrete beam till it reaches the limit state. The flexural and/or shear cracks appearing in the damaged state are then repaired by bonding composite patches and the repaired beam is load-tested again. Test results of such actual loading tests are then used to verify model predictions.

Since anchorage zone cracking is a commonly observed phenomenon in prestressed concrete beams, critical investigation of the end zone stresses of such beams is also aimed in this study, because such cracks tend to shorten the service life of such beams in exposed situations, as in the case of a highway bridge structure [1]. In exposed situations, such cracks tend to get wider as the embedded steel gets corroded.

Several past studies on anchor zone stresses in post-tensioned beams have been reported in the published literature. The earliest

* Corresponding author. Tel.: +1 615 322 7477; fax: +1 615 322 3365.
E-mail address: prodyot.k.basu@vanderbilt.edu (P.K. Basu).

[1] Author note. This manuscript is based on the doctoral dissertation research work conducted by the first author at Vanderbilt University Department of Civil and Environmental Engineering.

http://dx.doi.org/10.1016/j.engstruct.2015.07.018
0141-0296/

approaches as put forward by Magnel and Guyon treated the problem as two dimensional [2,3]. Several efforts followed these two studies viewing the same problem in the 3-D context [4–6]. A survey of previous studies did not reveal any significant effort leading to better understanding of the actual state of stress in the anchor zone or end region of, especially, pretensioned prestressed beams. Some of the early studies did, however, investigate the effects of vertical reinforcement in such regions for the prevention of horizontal cracks [7–11]. For instance, Padmarajaiah and Ramaswamy [9] undertook experimental studies on such beams incorporating short steel fibers as supplemental reinforcement. They also undertook nonlinear finite element analysis using the commercial software Ansys for predicting the load vs. deformation behavior, validating with the experimental data. Concrete was modeled with hexahedral solid elements using William and Warnke characterization and truss elements were used for steel. The interfacial bond effect was characterized by tangential linear spring elements located at the nodal points. The focus of the study was the influence of steel fibers on quasi-static load vs. deformation behavior of such beams. Another group of researchers [10] tried to improve the prediction using the layered beam approach. Markovic et al. put forward a computationally efficient analysis scheme for nonlinear analysis of such beams based on Euler–Bernoulli theory, smeared crack concept, tendon slippage and material softening accounted for by the arc-length method. The results appeared to follow the trend of experimental data available in the literature.

In modern prestressed concrete construction, the main approaches used for the control of stresses at the ends of pretensioned members, besides adding vertical reinforcement, have been – reducing eccentricity of the strands at the ends; deliberate debonding of selected strands with concrete at and near anchorage zones; introducing supplemental steel rods for reinforcement; adding top strands, which can be debonded in the center portion of the girder, as needed; releasing the strands when the concrete has reached higher compressive strength.

For better prediction of the state of stress and the nature of damage in the critical regions of pretensioned concrete beams, this study focuses on determining the state of stress in the end-zone of prestressed concrete beams using the proposed finite element modeling and simulation scheme so that more effective steps can be taken in the design to control such cracking.

As the pretensioned beams used in practice tend to be deep and slender, stress predictions, even away from the ends, based on conventional Euler–Bernoulli assumptions may not be valid in all cases. As a consequence, both ACI-318 [12] and AASHTO LRFD [13] recommend a simplistic semi-empirical approach called the strut-and-tie method for designing the secondary reinforcement, especially, near the anchor zone. The basic premise of the strut-and-tie method is that near limit state a complex structural member can be treated as an equivalent truss structure. Although the approximate representation of the limit state in the method makes sense, according to the recent studies, however, designs based on this method are found to be inefficient and overly conservative [14]. Since 1960's, finite element simulation to predict the response of prestressed concrete beams has been widely used. But some of the finite element models used for this purpose were grossly inadequate and were not representative of the real mechanics of prestressed concrete beams and most recent attempts to improve the situation [15–17] were not quite successful.

In their study, Ayoub and Filippou [15] implemented a mixed formulation based model to represent the prestressed concrete beam in the general purpose Finite Element Analysis Program (FEAP) [18]. The model of the prestressed concrete beam comprised of three components. First, a fiber beam-column element is used to represent the behavior of concrete and embedded reinforcement. Secondly, a 1-D truss element is used to represent the prestressing tendon. Finally, bond elements defined at the nodal points accounted for the transfer of interfacial forces between concrete and prestressing strand. The pretensioning operation is considered in two stages at discrete times. First, the pretension is induced in the tendons which is followed by the transfer of prestress to concrete. In the first stage of the analysis, only the 1-D tendon elements are active. Also for representing the bedding element, a linear stiff spring is used at one end of the tendon. The prestressing force is applied at the other end. In the second stage of analysis, the beam-column elements and bond elements are activated. Thereafter, the applied prestressing force in the tendon is reduced to zero, to simulate the release of the strands. The bedding element at the other end is also removed at the same time. In this stage, the prestressing force in the tendon element is transferred to the concrete fiber based beam-column elements via the idealized bond elements. This study makes a number of sweeping assumptions which may have questionable validity. First, 1-D representation of the tendon ignores one of the main stress transfer mechanisms between the strand and the concrete which is 3-D in nature. This mechanism is called wedge effect or "Hoyer effect". This is caused by the tendency of the strand to return to its original size from the reduced diameter resulting from the initial pretensioning force (Fig. 1). Also, the model does not adequately account for cracking and tension stiffening effects.

As an attempt to further unravel the important issues of finite element modeling of prestressed beams, Arab et al. [16] used the Concrete Damaged Plasticity (CDP) model in the commercial software 'Abaqus' [19]. In modeling the interaction between the prestressing strand and the concrete, Arab, et al. tried two methods, terming them as (a) the extrusion technique, and (b) the embedment technique. In the first technique, a coefficient of friction is used to define the tangential behavior and hard contact is used for normal behavior. While preventing penetration between steel and concrete, the hard contact model prevented tensile stress transfer through interfacial interaction. In the embedment technique, however, the prestressing strands are assumed to be embedded into the concrete matrix with the prestressing strands modeled by 1-D truss elements and the concrete matrix by solid elements. In the interface model, the degrees of freedom of the prestressing strand element nodes are supposedly constrained with respect to the interpolated values of the corresponding degrees of freedom of the concrete host elements.

Arab et al. also used a steel casting bed model to provide support to the beam without restraining longitudinal and transverse movements. The interface between the casting bed and the beam is assumed to be frictionless and of hard contact type, allowing for separation. Pretensioning is accomplished in two steps. In the first step, the strands are pretensioned and no relationship is established between strand and concrete. In the second step, the strain-compatibility is applied between strand and concrete to simulate release of the strands.

Acute lack of accuracy of the predictions by this model may be attributed to some of the assumptions made by Arab et al., appearing to defy the basic mechanics of the problem. For instance, the assumption of strain compatibility at steel and concrete interface in both extrusion and embedment techniques do not appropriately allow for the possibility of slippage due to bond failure. Another area of concern centers on the mesh. The elements around the prestressing strand appear to have quite high aspect ratios and this is expected to introduce errors in representing the interfacial bond behavior. For numerical stability, according to the contact sub-module of Abaqus [19], the concrete matrix at the interface should have been meshed finer than the strand, which is contrary to the model used by Arab et al. Furthermore, the experimental

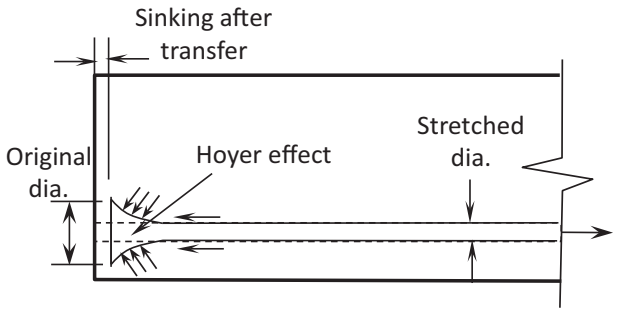

Fig. 1. Strand diameter after release showing wedging at the end.

data used for verification purposes were taken from Akhnoukh [20] as variation of "nominal axial strain" along the length of the beam. This validation attempt can at best be termed as qualitative or "trend" comparison, rather than actual quantitative comparison. Also, the experimental data were based on surface strain measurements using mechanical (DEMEC) gage readings, a very crude tool for point wise strain measurement.

The 2012 study by Okumus et al. [17] is also based on modeling with Abaqus. The concrete material is again represented by using CDP model. Justifying computational efficiency, this nonlinear material model was used only for the end regions of the beam. This study makes a slew of simplifying and, sometimes unreasonable assumptions resulting in a model which fails to simulate the real behavior. The reinforcing rods are modeled with 1-D elements and are embedded in the concrete matrix. The presence of prestressing strands are ignored. Instead, the prestressing force is applied directly to the concrete as surface loads, along the transfer length, around the perimeter of the strands. In Okumus et al.'s study, it has been stated that the bond stresses and transfer lengths used to define the prestressing forces, are obtained from O'Callaghan's [21] experimental measurements via strain gages placed on the strands. However, in O'Callaghan's study there is no information about the bond stresses and the transfer lengths of the strands. Additionally, it is not possible to obtain this type of data accurately by placing just a few strain gages on the strands. Also, the Hoyer effect is missing, as no strands were used.

Herein after, all the three problems considered by Ayoub, Arab et al. and Okumus et al. [15–17] will be called problems of references 15, 16 and 17, respectively. As part of this study, these three problems are modeled and re-simulated by the authors, using the proposed finite element modeling scheme. Later in this study, the results obtained with the proposed approach is compared with the numerical results presented in these references and the experimental data used therein, so that the advantages of the proposed scheme can be established.

2. Proposed modeling scheme

The proposed modeling scheme is now explained with the help of a test pretensioned concrete beam which was actually fabricated and laboratory tested to failure, as part of this study. This small scale test beam was designed by a licensed Tennessee Department of Transportation (TDOT) engineer by following AASHTO LRFD design guidelines [13]. The beam was designed to withstand a total limit load of 99 kN's. During the design process, factors like ease of handling, nature of the experiments to be performed and limitations of the fabrication and testing facilities in the laboratory were taken into account. The details of the test prestressed concrete beam are shown in Fig. 2. Grade 60 reinforcing rods of 9.53 mm (#3) and 5.08 mm (#2) diameters are used as the top hanger bars and stirrups, respectively. At the bottom of the beam, two 12.70 mm diameter low-relaxation prestressing strands with an ultimate tensile strength of 1862 MPa are placed. The total length of the beam is 2590.8 mm. As shown in Fig. 3, the beam was tested under four-point bending condition.

Taking advantage of symmetry, the test prestressed beam is modeled using half of the beam length. The strands and the reinforcements are modeled using equivalent rectangular cross sections. This allowed simplification and easy optimization of the interfacial mesh shapes of the concrete and the steel elements. This is an unavoidable concern of using linear-tetrahedral elements on a curved surface. The stirrups of the beam did not form a closed loop, so based on experience with trial simulations, the stirrups were ignored in the model. This allowed computational efficiency without sacrificing accuracy till the limit state is reached.

To prevent the unrealistic concentration of stresses at supposedly knife-edge supports, such locations of the model were represented by narrow strips to more closely simulate the actual condition. Likewise, the applied loads were defined as pressure loads over narrow strips instead of sharp line loading. During the meshing process, at steel–concrete interface, concrete was treated as the slave surface and was meshed finer than steel, ensuring proper convergence of the solution. Modeling and simulation of the beam was undertaken in the following three steps.

Step 1: To simulate initial prestressing of strands before pouring of concrete, the strands are first tensioned without allowing for any bond with concrete (Fig. 4). This is accomplished by defining an interaction with normal behavior with hard contact between concrete and strand. This prevented inter-penetration between strand and concrete. This condition simulates initial prestressing of strands before pouring of concrete, as evidenced by the state of stress shown in Fig. 4 signifying unstressed condition of concrete.

The behavior of concrete is represented by using the Plasticity–Damage (PD) model which is a variation of Drucker–Prager criterion. In the case of polycrystallines, material models based on plasticity theories alone work well wherein the dominant mode of damage is governed by the slip process. Attempts to model concrete and quasi-brittle materials based on such plasticity theories leading to a failure surface which included pressure sensitivity, strain-hardening, etc., was not successful. In the other extreme, the use of models based on continuum damage theory, which accounts for micro-cracking and strain softening, alone could not also fully represent the observed mechanical behavior of concrete. The concrete material is characterized by a-priori presence of micro-cracks which tend to propagate and coalesce after load application, leading to drop in strength and degradation of physical properties. It is evident from typical uniaxial stress vs. strain response of concrete, as shown in Fig. 5, that the nonlinear response of concrete actually includes both plastic behavior in the hardening region and damage through stiffness degradation in the softening region, causing irreversible deformations. Allowing for such combined effect can conveniently be based on assumptions of isotropic hardening and isotropic damage, as explained in the following. The combination can be effective-stress based, as followed by Lee and Fenves [22] with the effective-stress being defined in terms of the average micro-scale stress acting on the undamaged material.

It is important to allow for different responses of concrete in tension and compression [23] and associated stiffness degradation in terms of two damage and hardening variables. To characterize stiffness degradation, a damage variable can be introduced in the context of Kachanov [24] in terms of an isotropic damage variable based essentially on specific damaged surface area. The

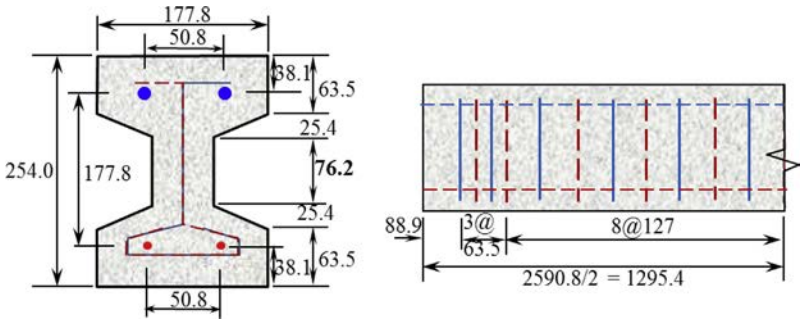

(a) Details of cross-section (b) Stirrups

Fig. 2. Details of prestressed concrete test beam (mm).

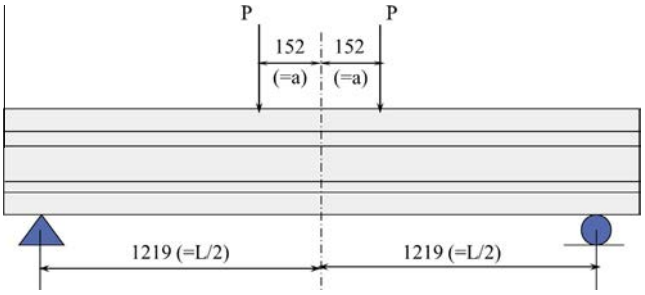

Fig. 3. Applied loading configuration of the test beam (mm).

elasto-plastic constitutive relationship for the yield surface, allowing for the separate evolution of tensile and compressive strengths, can be decoupled from considerations of stiffness degradation. In the case of concrete materials, the resulting material model can be based on infinitesimal deformations. Also, for the present problem, low confining pressure and in-significant strain-rate dependence can be assumed.

As shown in Fig. 5, the total strain tensor, ε_{ij}, will have an elastic component, ε^e_{ij}, and a plastic component, ε^p_{ij}. In the context of Kachanov [24], if d is the scalar stiffness degradation parameter, with $0 \leqslant d \leqslant 1$, the constitutive equation in a 3-D stress field can be represented by Eq. (1) below:

$$\sigma_{ij} = C^e_{ijkl} : \left(\varepsilon_{kl} - \varepsilon^p_{kl}\right) \tag{1}$$

where the degraded elastic stiffness tensor of rank four, C^e_{ijkl} is represented by Eq. (2):

$$C^e_{ijkl} = (1 - d) \cdot C^{eo}_{ijkl} \tag{2}$$

C^{eo}_{ijkl} is the initial elastic stiffness tensor; and σ_{ij} is the Cauchy stress tensor. The effective stress tensor $\bar{\sigma}_{ij}$ can now be defined by Eq. (3) as

$$\bar{\sigma}_{ij} = \frac{\sigma_{ij}}{1 - d} \tag{3}$$

To account for different damage effects in tension and compression, multi-softening as well as multi-hardening yield functions need to be used. Due to noticeable difference in the ultimate strength in tension (f_t) and compression (f_c), the yield function in terms of effective stress can be defined by using Eq. (4) below:

$$F\left(\bar{\sigma}_{ij}, \bar{f}_t, \bar{f}_c\right) \leq 0 \tag{4}$$

with effective stress responses $\bar{f}_t = \frac{f_t}{1-d}$ and $\bar{f}_c = \frac{f_c}{1-d}$, where $d = 1 - (1 - d_c) \cdot (1 - d_t)$, d_c being the damage parameter in compression and d_t in tension, while $0 \geqslant d_c$, $0 \geqslant d_t$. Thus, one damage parameter, d, can be used to represent the combination of tensile and compressive damages. The individual damage parameters, d_c and d_t, can be represented in terms of a hardening variable $\tilde{\varepsilon}_c$ and a softening variable $\tilde{\varepsilon}_t$, related to the dissipation of energy during the damage process. Such representation works fine in the case of

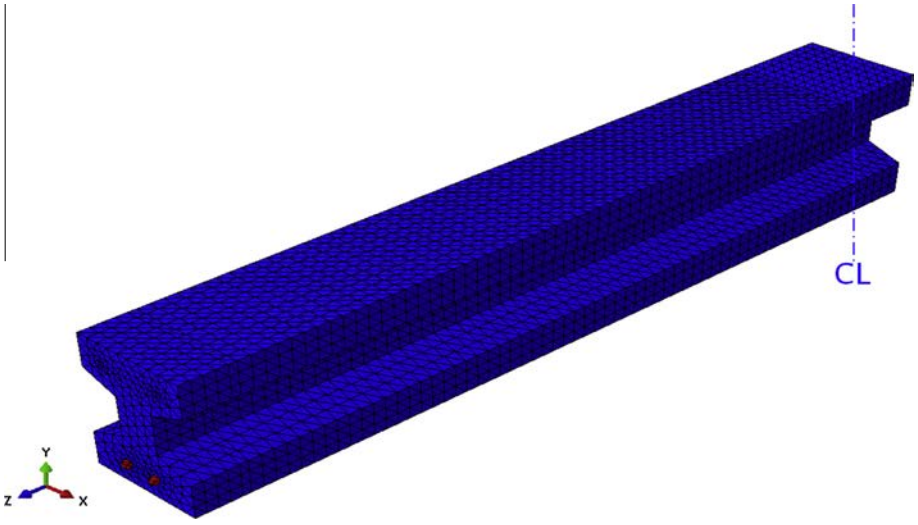

Fig. 4. Unbonded strands are stretched to initial prestressing force level.

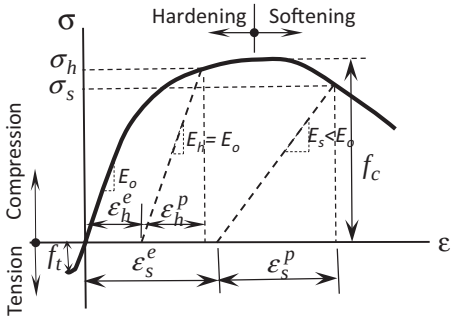

Fig. 5. PD model definition of compressive stress vs. strain relationship of concrete.

monotonic loading. For rate-independent plasticity and inviscid plastic damage, the yield surface can then be conveniently represented by Eq. (5):

$$\overline{F}(I_1, J_2, J_3, \tilde{\varepsilon}_c, \tilde{\varepsilon}_t) \le 0 \tag{5}$$

where $\overline{F}$ is a function of the first invariant of Cauchy stress tensor as well as the second and third invariants of deviatoric part of the effective stress tensor defined as $\bar{I}_1 = \bar{\sigma}_{ij} \cdot \delta_{ij}$; $\bar{J}_2 = 1/2 \cdot \bar{S}_{ij} \cdot \bar{S}_{ij}$; $\bar{J}_3 = 1/3 \cdot \bar{S}_{ij} \cdot \bar{S}_{jk} \cdot \bar{S}_{ki}$ where $\bar{S}_{ij} = \bar{\sigma}_{ij} - \delta_{ij} \cdot \frac{\bar{I}_1}{3}$. For low confining pressures, the parameter $\bar{J}_3$ can be dropped from the expression (Eq. (3)) for yield surface.

The plastic flow defined in terms of a plastic flow potential function, $g(\bar{\sigma}_{ij})$, based on non-associative flow rule, is a function of the effective stress tensor, as shown in Eq. (6) below.

$$d\varepsilon^p = d\lambda \frac{\partial g(\bar{\sigma}_{ij})}{\partial \bar{\sigma}_{ij}} \tag{6}$$

Here $d\lambda$ is a non-negative parameter which may vary throughout the loading history and $d\varepsilon_p$ denotes the plastic strain increment, and $\partial g/\partial \bar{\sigma}_{ij}$ represents plastic flow, not necessarily normal to the failure surface. For the preceding relationships, the following conditions hold,

$$\overline{F} \le 0; \quad d\lambda \ge 0; \quad d\lambda \overline{F} = 0$$

The flow potential g, when expressed in terms of Drucker–Prager hyperbolic function, can be represented by Eq. (7) in the following form:

$$g = \sqrt{(m f_t \cdot \tan\psi)^2 + 3\bar{J}_2} - \frac{\bar{I}_1}{3} \cdot \tan\psi \tag{7}$$

Table 1
Plasticity parameters of concrete in finite element model.

Parameter	Value
Dilation angle (ψ)	31°
Eccentricity (m)	0.1
Ratio of initial equi-biaxial compressive yield stress to initial uniaxial compressive yield stress (f_{bo}/f_c)	1.16
Ratio of the second stress invariant on the tensile meridian to the compressive meridian ($\rho_t/\rho_c = K_c$)	0.667
Viscosity parameter (default – no effect)	0.001

In which, f_t is the uniaxial tensile strength of concrete, ψ is dilation angle, and m is a parameter representing the eccentricity of the plastic potential surface.

Following the methods of Lee and Fenves [22],

$$d\tilde{\varepsilon}^p = \begin{Bmatrix} d\tilde{\varepsilon}_t^p \\ d\tilde{\varepsilon}_c^p \end{Bmatrix} = \begin{bmatrix} r(\hat{\sigma}) & 0 & 0 \\ 0 & 0 & -(1 - r\hat{\sigma}) \end{bmatrix} \cdot \begin{Bmatrix} d\hat{\varepsilon}_1 \\ d\hat{\varepsilon}_2 \\ D\hat{\varepsilon}_3 \end{Bmatrix} = \hat{h}(\hat{\sigma}, \hat{\varepsilon}^p) \cdot d\hat{\varepsilon}^p \tag{8}$$

Here, the stress weight factor, $r(\hat{\bar{\sigma}}) = \frac{\frac{1}{2}\sum_{i=1}^{3}(|\hat{\bar{\sigma}}_i| + \hat{\bar{\sigma}}_i)}{\sum_{i=1}^{3}|\hat{\bar{\sigma}}_i|}; 0 \le r(\hat{\bar{\sigma}}) \le 1.$

The corresponding yield condition can be shown to take the form:

$$\overline{F} = \frac{1}{1-\alpha}\left(\sqrt{3\bar{J}_2} - \alpha\bar{I}_1 + \beta\tilde{\varepsilon}^p\hat{\bar{\sigma}}_{\max} - \gamma\hat{\bar{\sigma}}_{\min}\right) - \bar{\sigma}_c\hat{\tilde{\varepsilon}}_c^p \le 0 \tag{9}$$

Here, $\alpha = \frac{(f_{bo} - f_c)}{(2f_{bo} - f_c)}$ with f_{bo} as the biaxial compressive strength with the ratio f_{bo}/f_c often taken as 1.16; $\beta = \frac{\bar{\sigma}_c(\tilde{\varepsilon}_c^p)}{\bar{\sigma}_t(\tilde{\varepsilon}_t^p)}(1-\alpha) + (1+\alpha)$ with $\bar{\sigma}_c$, $\bar{\sigma}_t$ being effective compressive and tensile cohesive stresses and the parameter $\gamma = \frac{3(f_{to} - f_{bo})}{(2f_{bo} - f_{to})}$ with f_{to} as the triaxial compressive strength. The biaxial and triaxial compressive strengths are based on isotropic states of stress.

The value of α range over 0.08–0.12, and for γ the typical value is close to 3 [19]. The Eq's. (6)–(9) were used in modeling the concrete in the prestressed concrete beam. Typical views of a meridian of the yield surface and sectional view of octahedral plane are shown in Fig. 6, where ρ_c and ρ_t are the radial distance $\left(\sqrt{2J_2}\right)$ of critical points on the octahedral plane for compression and tension failures corresponding to a particular value of isostatic pressure $I_1/3$.

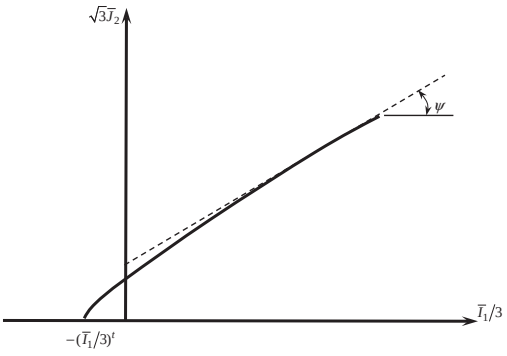

(a) Shape of meridian of failure surface

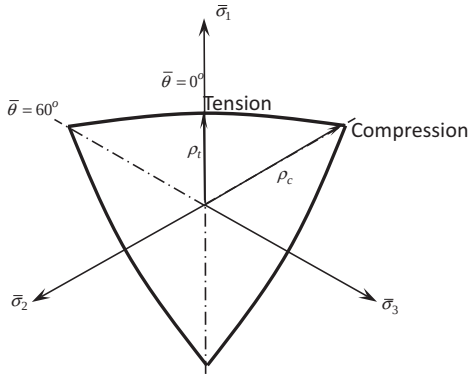

(b) Typical deviatoric section of failure surface

Fig. 6. PD failure surface for concrete.

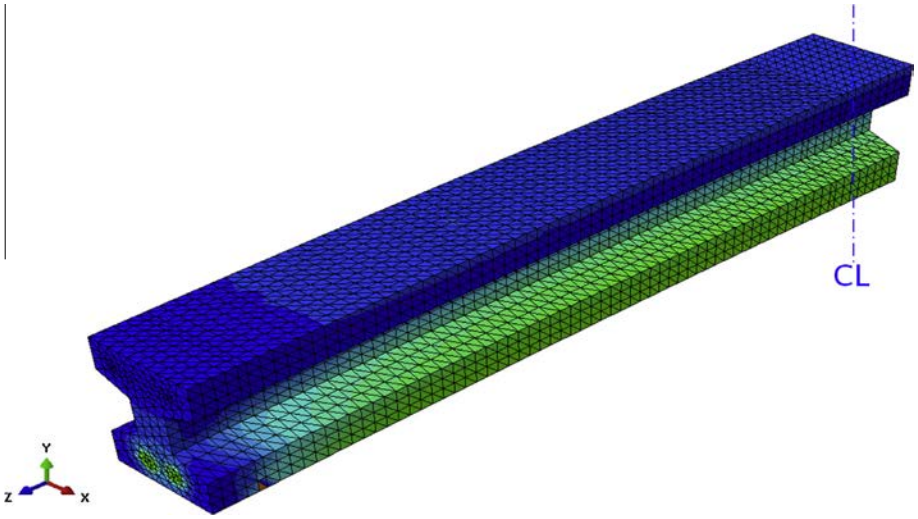

Fig. 7. Strands are bonded to concrete followed by releasing of the strands.

Table 2
Bond parameters of reinforcing rod.

Parameter	Value
Stiffness of interfacial spring elements (K)	19,064 N/mm
Coefficient of friction (k)	0.4
Normal behavior	Hard contact
Maximum separation for damage initiation	0.42 mm
Total/Plastic displacement	25.4 mm
Damage evolution exponential parameter	4.3

Table 3
Bond parameters of strand.

Parameter	Value
Stiffness of interfacial spring elements (K)	47884 N/mm
Coefficient of friction (k)	0.4
Normal behavior	Hard contact
Maximum separation for damage initiation	0.42 mm
Total/Plastic displacement (for bond failure)	25.4 mm
Damage evolution exponential parameter	4.3

In the absence of actual test data, the compressive behavior of concrete is often defined by Hognestad et al.'s [25] stress vs. strain relationship for concrete. The ultimate compressive strength of concrete was determined by conducting unconfined compression tests on concrete cylinders. Based on experimental results, the ultimate compressive strength of concrete used for the simulation was taken as 44.8 MPa. The crushing strain of concrete was found to be close to 0.003. The modulus of elasticity and tensile strength of concrete shown below are based on standard ACI formulas and were close to the measured values [12]:

$$E_c = 4700\sqrt{f_c} = 31,685 \text{ MPa} \tag{10}$$

$$f_{ct} = 0.33\sqrt{f_c} = 4.17 \text{ MPa} \tag{11}$$

Tension stiffening action in concrete is represented by using the built-in fracture energy cracking criterion. The fracture energy of concrete is determined by conducting a regression analysis of the experimental results and the recommended values in the literature [19,26–28]. The value of the fracture energy of concrete used in the finite element simulation is 121 N/m. The summary of the other plasticity parameters used for the plasticity–damage model is shown in Table 1. These values are standard for the concrete used in the study. The choice of the viscosity parameter (0.001) was solely based on the consideration of its beneficial effect on the rate of convergence of the solution with hardly any effect on the quality of the solution.

Step 2: Unlike concrete, the tensile and compressive strengths of all embedded steel can be assumed to be the same. The stress vs. strain curve of prestressing steel does not have a well-defined yield point and approximations of bilinear or elastic–plastic variations are not uncommon. For defining the composite action between the two material phases, the mechanism of mutual transfer of forces through the interface needs to be defined appropriately.

The main mechanisms involved in the process are identified as adhesion, friction, and mechanical interlock action. The component due to adhesion can be attributed to chemical bonding as well as the stresses created during the setting and hardening processes of concrete. Adhesion and friction are important in the case of steel without indentation like surface roughness. Otherwise, the mechanical locking process also becomes important. In this study, the steel used were not ribbed and the consideration of interfacial behavior is limited to bond-slip behavior idealized by using interfacial distributed spring elements of zero dimensions to transfer normal and tangential forces at the interface. The stiffnesses of interface elements allowing for slippage due to stiffness degradation and complete separation, are based on actual test data of pull-out tests. Although a number of more complex damage models at and the vicinity of interface have been put forward, but will not be considered here. In the other extreme, some researchers assumed full bond between the two phases.

After the interfacial bond is restored between strand and concrete, the externally applied strand forces are removed. This condition simulates the release of strands to transfer the prestress after the concrete has gained the desired strength (Fig. 7). To achieve higher accuracy, all the rebar and the prestressing strands are modeled with 3-D solid elements. Also, the constitutive properties of reinforcing steel and prestressing strand were represented by nonlinear elasto-plastic material models. The material model for the strand is taken from the PCI Design Handbook [29]. The material model for steel reinforcement, the interfacial bond parameters between concrete, strand and rebar were based on further

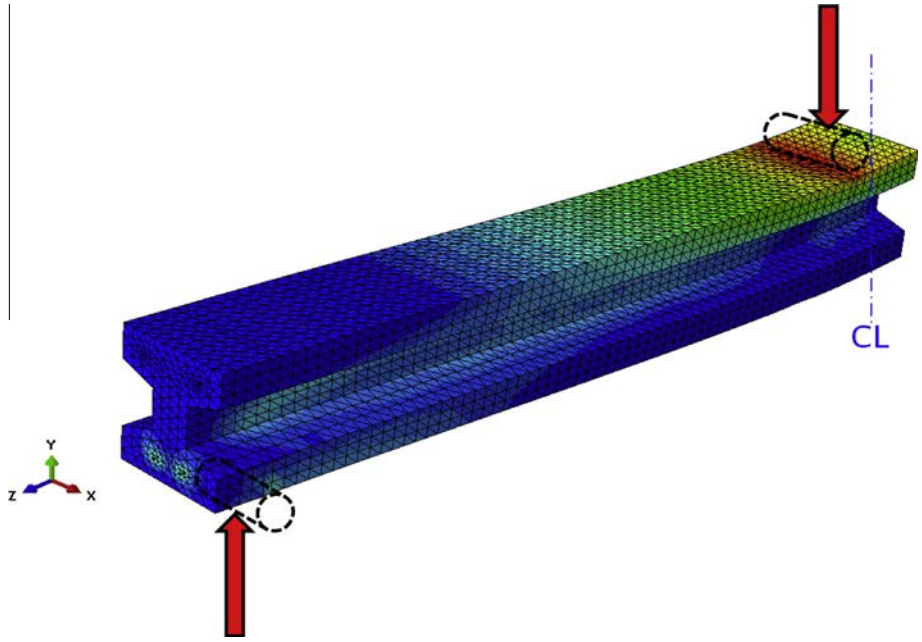

Fig. 8. Effect of external load application on the test beam.

Table 4
Bond parameters of adhesive.

Parameter	Value
Stiffness of interfacial spring elements (K)	60558 N/mm
Maximum separation for damage initiation in normal direction	0.137185 mm
Total/Plastic displacement	0.146354 mm
Damage evolution exponential parameter	Linear

experimental studies undertaken by the author and correlated with data in [30,31].

The bond between the concrete and the strands are modeled using the hard contact normal behavior described earlier coupled with the friction-governed tangential behavior, the cohesive behavior, and the damage behavior. The friction-governed tangential behavior is used to represent the increased bond force between the strands and the concrete. The pressure on the strands exerted by the concrete is higher at the parts of the beam which are closer to the supports and load points. Therefore, the friction between the concrete and the strands is variable along the beam and this phenomenon is taken into account by using friction-governed tangential behavior as previously mentioned. The cohesive behavior is included in this step to take into account the slippage between the concrete and the strands through the whole length of the beam. Finally, the damage behavior governs the degradation of the cohesive stiffness values after a critical bond stress (or critical slippage displacement) is reached, until finally the bond can support no load. Also, the wedging effect and the Poisson radial

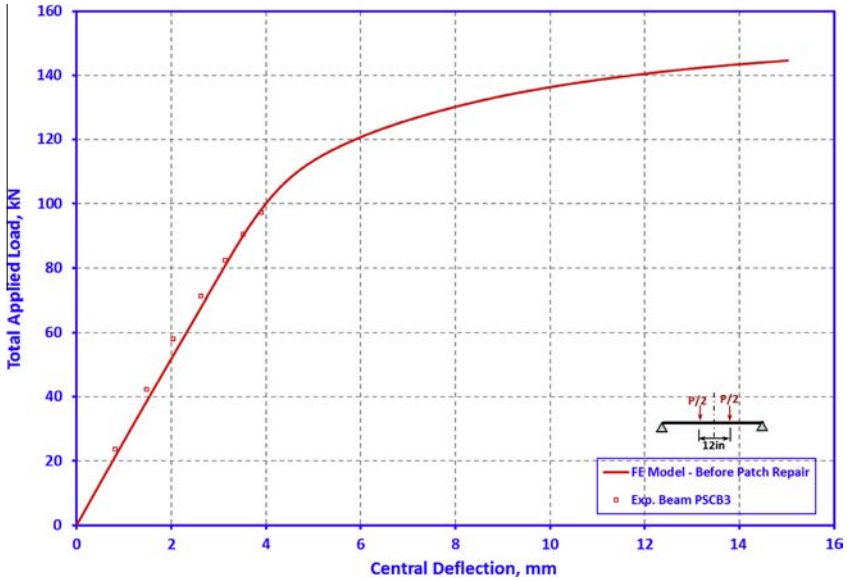

Fig. 9. Variation of central deflection with applied load for test beam before patch repair.

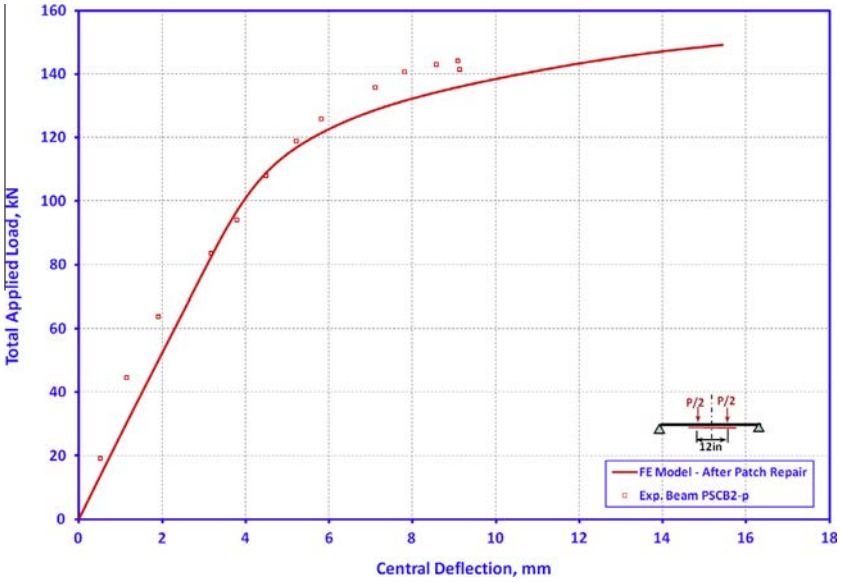

Fig. 10. Variation of central deflection with applied load for test beam after patch repair.

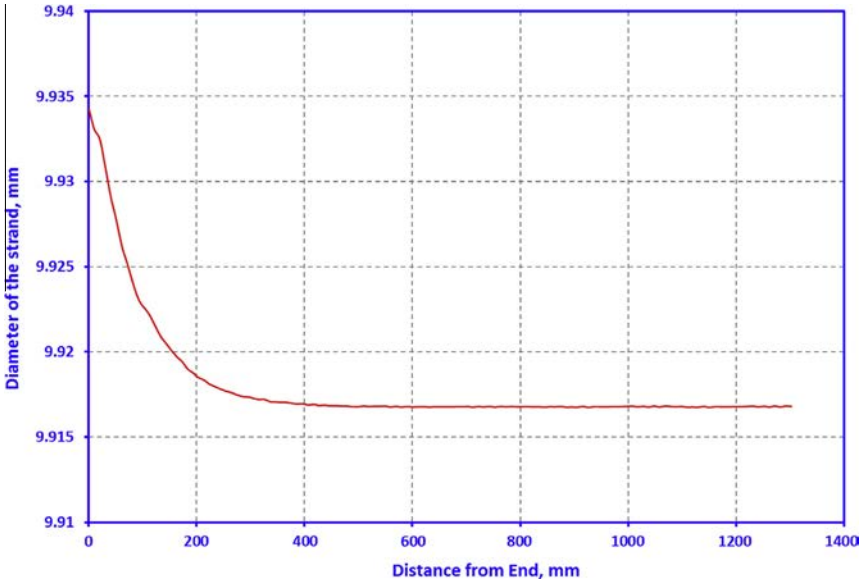

Fig. 11. Variation of strand diameter along the beam length, at the end of Step 2.

expansion are automatically taken into account by the model. The summary of the bond parameters used for the bond model of rebar and strand are shown in Tables 2 and 3, respectively.

Step 3: The beam is subjected to external loads and then analyzed to determine the response quantities of interest. This loading may refer to the service condition (Fig. 8). As in Step 2, the same interaction and material models were used in Step 3 analysis.

3. Experimental studies of test beam

The experimental work performed with the test beam was divided in two stages: (1) during the first stage, the beam was four-point loaded past the service load, to cause initial damage in the form of structural cracks, and (2) in the second stage, the damage created in Stage 1 is repaired with bonded composite patch and then loaded again until failure. For the composite patch repair material, Sika Carbodur and its matching adhesive Sikadur 30 were used.

Since there is lack of standardization of test procedures for determining the properties of composite materials and adhesives, new experimental methods has to be developed in the context of this research [32]. The flexural patch repair of the test beam was done by bonding a 101.6 mm × 457.2 mm FRP composite strip (Carbodur) at the bottom face with specified adhesive (Sikadur 30). The thickness of the composite strip is 1.19 mm with the breaking strength and tensile modulus determined as 3096 MPa and 164,785 MPa, respectively. The adhesive was modeled by using the cohesive bond and damage sub-modules of Abaqus. Summary of the bond parameters used for modeling the adhesive is shown in Table 4. More information can be found in [33].

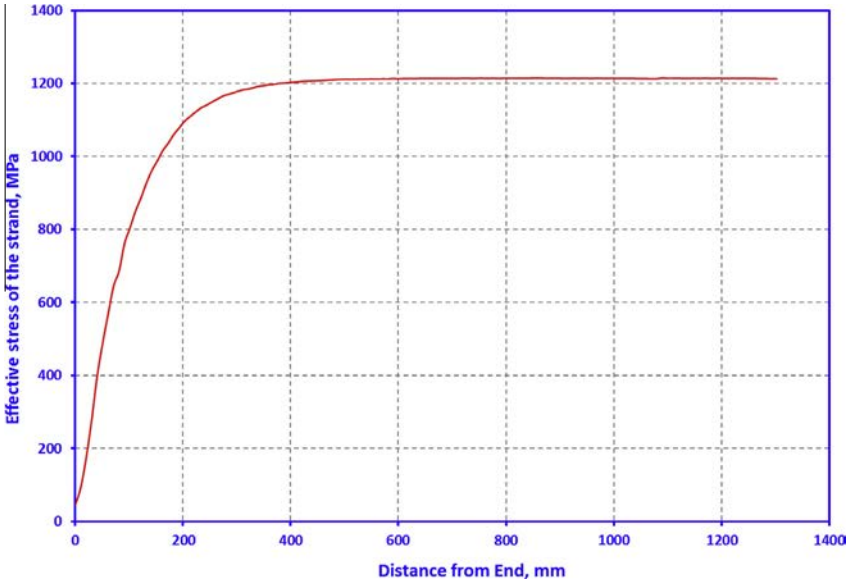

Fig. 12. Variation of the effective stress of the strand vs. distance from end.

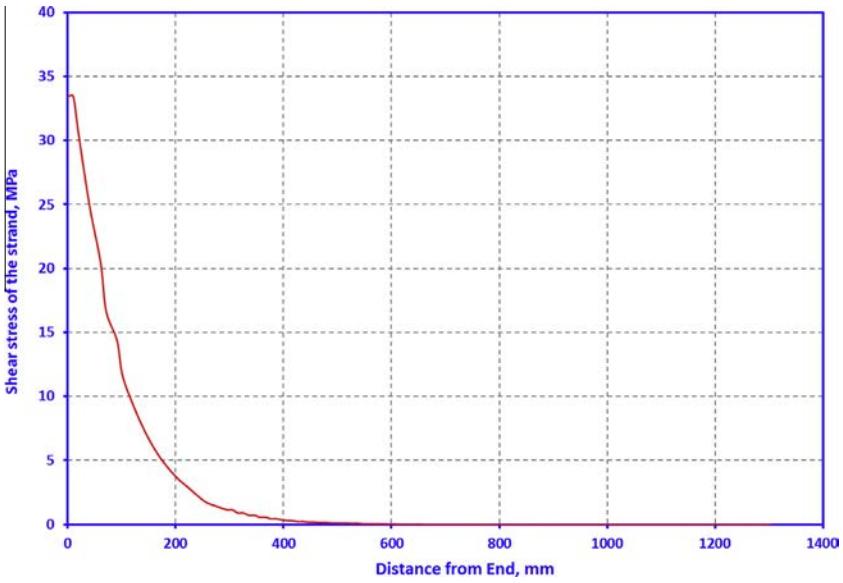

Fig. 13. Variation of shear bond stress of strand along the beam length.

3.1. Finite element analysis of test beam

Finite element analysis of test prestressed concrete beam, before and after patch repair, was undertaken using Abaqus as the primary analysis tool based on the PD Model and the bond-slip failure model discussed earlier. For this purpose, the relevant parts of the material model were modified using UMAT subroutines written in Fortran language. In the analysis, the three step-scheme defined earlier was faithfully followed. Proper characterization of the properties of concrete, namely, tensile, compressive and bond behaviors was extremely important for reproducing the real life response in modeling and simulation. Therefore every material and bond model used in this study is based on the results of the procedures already presented in the previous section.

4. Results of test beam

The flexural damage in the beam appeared near the center of the beam as a vertical crack in the bottom. After patch repair of this cracked beam, the limiting test load of the beam was found to be 134 kN. After developing some additional flexure cracks of small size, the repaired beam finally failed in shear. The original beam was designed to withstand 52.8 kN m, but the patch-repaired beam withstood roughly 71.5 kN m. This 36% improvement of capacity is significant. Finite element results for virgin and patch-repaired test beam are shown in Figs. 9 and 10. Test results as well as finite element simulation results as load vs. displacement plots show excellent agreement with finite element predictions. In the case of test results shown in Fig. 9, the loading was discontinued at a load level of 100 kN, to avoid excessive cracking

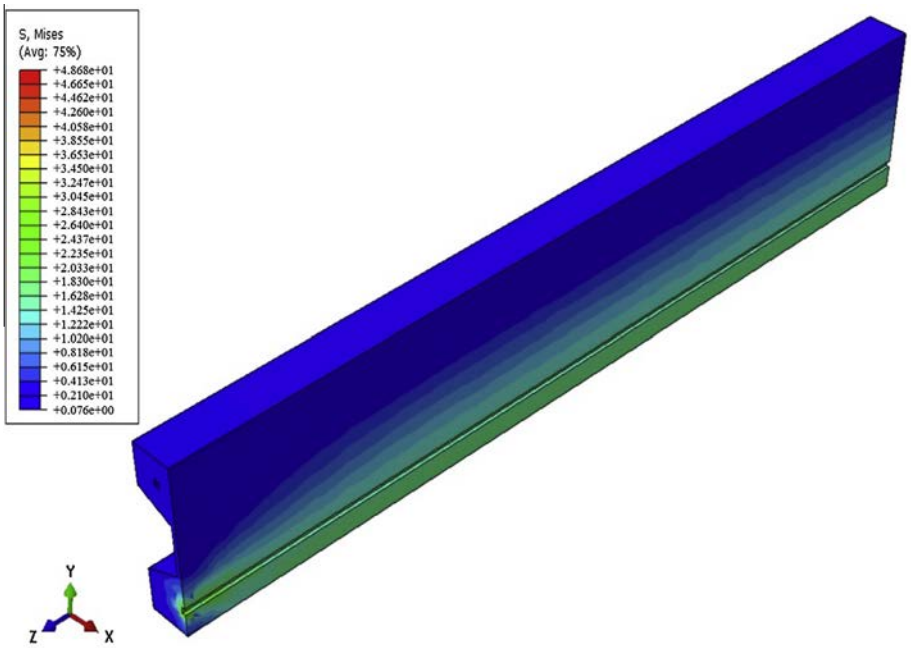

Fig. 14. Equivalent stress fringes at the end of Step 2 before patch repair (MPa).

and catastrophic failure. On the other hand, the after repair test results shown in Fig. 10 reflect that the test was continued till the deflection became excessive. During finite element simulation, in both cases the loading was continued till complete collapse. Consequently, as expected predictions show more ductile behavior near the collapse load. Small discrepancy between the test data and predictions of bonded patch repair beam is caused due to lack of experience in quality control of the repair process.

It was pointed out that, in a pretensioned beam, there are four main mechanisms taking place in the stress transfer process between the strand and the concrete – adhesion and friction between the concrete and the strand, mechanical resistance from helical shape of strand, and the end wedging effect. All these were allowed for in the finite element model. Fig. 11 shows the plot of diameter of the strand vs. distance at the end of the 2nd step – after the concrete has gained the design strength and the strands have been released. From this plot, one can easily conclude that the proposed model accurately accounts for the Hoyer effect. This aspect was further verified by examining the enlarged view of the plot near the end of the beam.

In the transfer of forces from the strand to the concrete with pretensioning, the transfer length is an important parameter. This length is the distance from the end of the beam to the point where the effective stress of the strand has developed fully. Although it is the usual design practice to assume that the variation of the prestressing force along the length of the beam is linear;

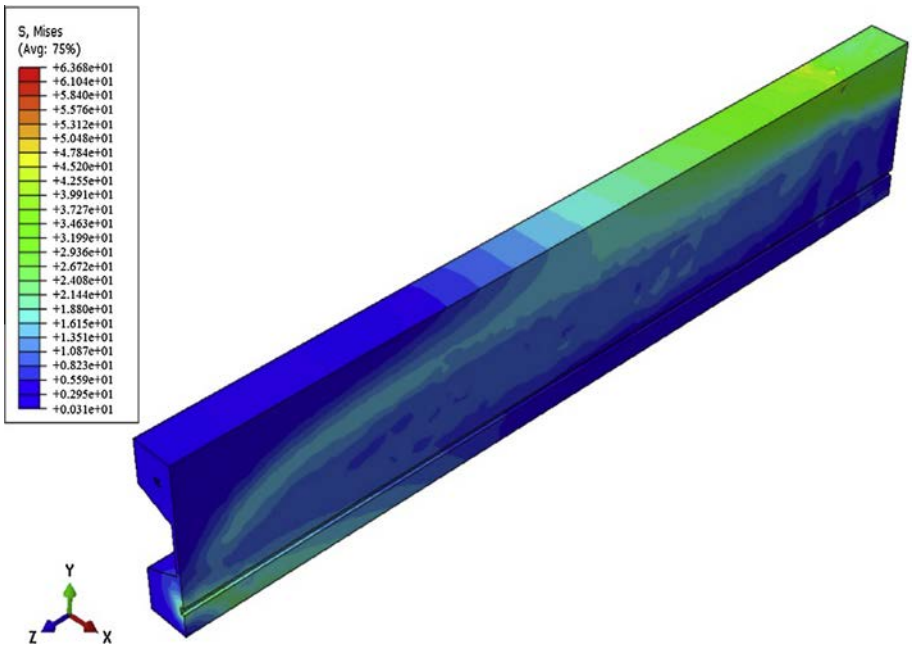

Fig. 15. Equivalent stress fringes at the end of Step 3 before patch repair (MPa).

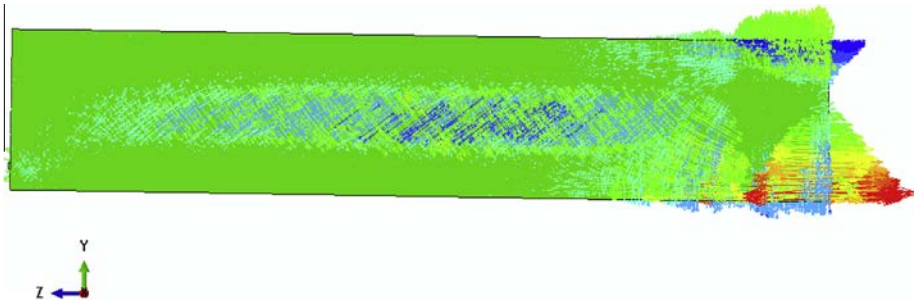

Fig. 16. Principal plastic tensile strains and their directions before patch repair.

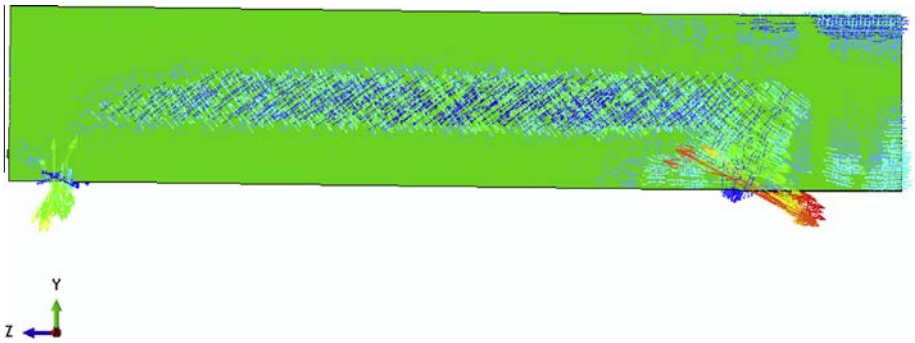

Fig. 17. Principal plastic tensile strains and their directions after patch repair.

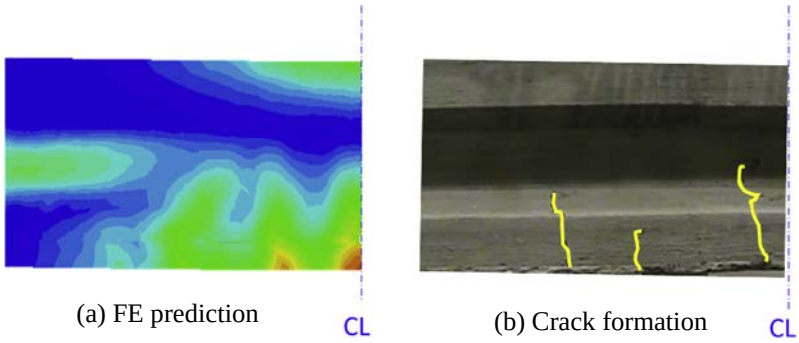

Fig. 18. Crack formation and principal plastic strain predictions before repair.

the actual variation is, however, a curve of approximately hyperbolic shape [34]. The stresses developed along the length of the strand at the end of Step 2 are presented in Fig. 12. This figure clearly shows that the variation of strand stress indeed follows a hyperbolic profile and that the transfer length is close to 500 mm or about forty times the strand diameter. The corresponding variation of the strand bond shear stress along the length of the beam which is shown in Fig. 13 identifies the transfer length, again, as 500 mm.

As previously stated, in the proposed finite element analysis scheme, all the stress transfer mechanisms are accounted for realistically. The good agreement between the finite element simulation results and the experimental data presented in Figs. 9 and 10 along with the realistic representation of stress transfer process validates this fact. Therefore, it can be stated that the proposed finite element scheme may serve as an effective tool to accurately determine the state of stress at the end zones of a pretensioned concrete girder, after the load transfer. The nature of distribution of equivalent stress fringes shown in Fig. 14 after the release of strands and the presence of smaller stress magnitudes near the ends caused by strand slippage are also evident. Moreover, the maximum stress contours around the strand resembles a hyperbolic curve which also agrees with published data on same [34]. The stress fringes shown in Fig. 15 are from four-point-bending test simulating the service load condition corresponding to the limit state. In Fig. 15, equivalent stress fringes depict that the highest stresses are localized at the loading points and support locations, although the stress-field around the strands caused by the prestress hardly changes.

The principal plastic tensile strains and their directions help locate the formation of cracks [19]. Figs. 16 and 17 present the principal plastic tensile strains and their directions before patch repair and after patch repair, respectively. As previously mentioned, during the Stage 1 loading test the beam underwent cracking in flexure only. Thereafter, during testing of the patch repaired beam, a new flexural crack appeared very close to the repaired region, but eventually the beam failed in shear. The principal plastic strains shown in Fig. 16 (before repair) and Fig. 17 (after repair) showed that the observed flexural and shear cracks during the tests appeared at critical locations as predicted in these figures. This makes sense because as per the study of Lubliner et al. [23], cracks form at locations where the maximum principal plastic

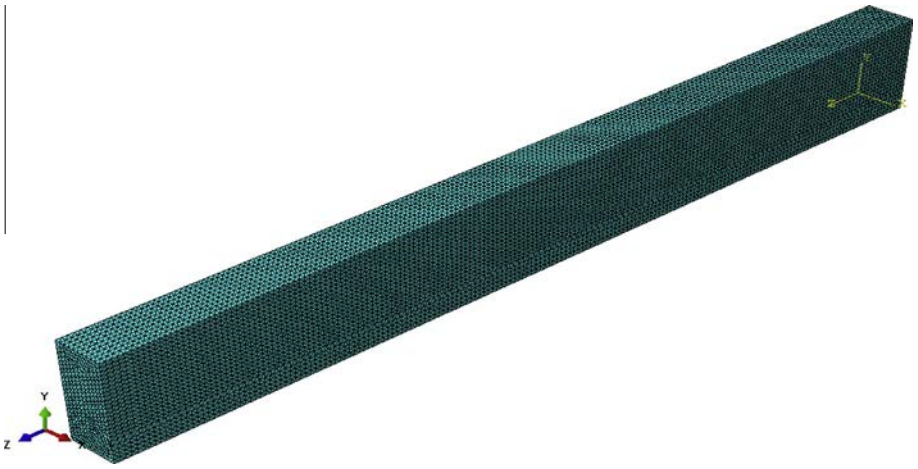

Fig. 19. FE Model (1/4th) for Ref. [15] problem.

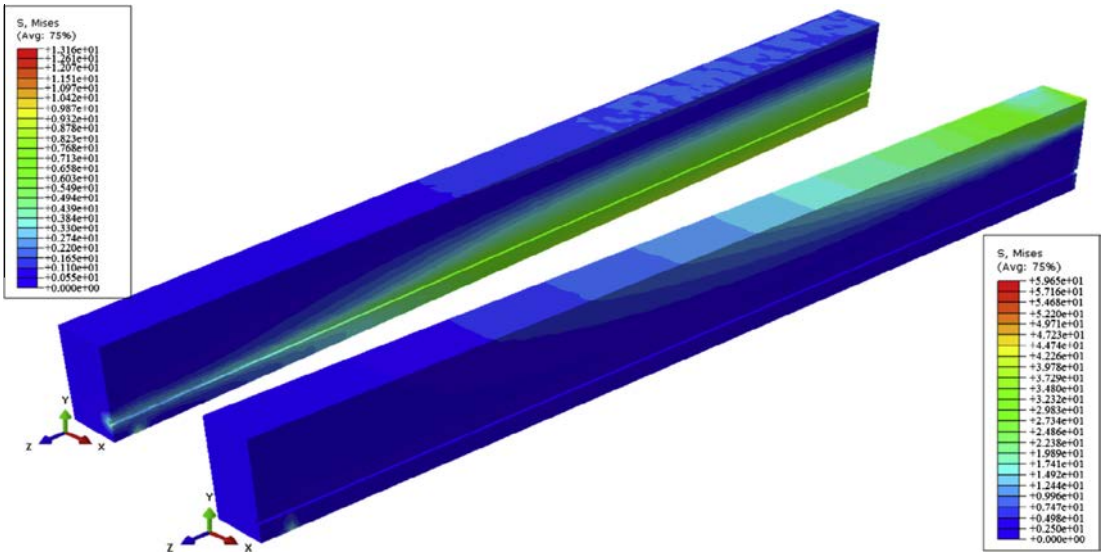

Fig. 20. Equivalent stress fringes at transfer (L) and at limit state (R), Ref. [15] problem (MPa).

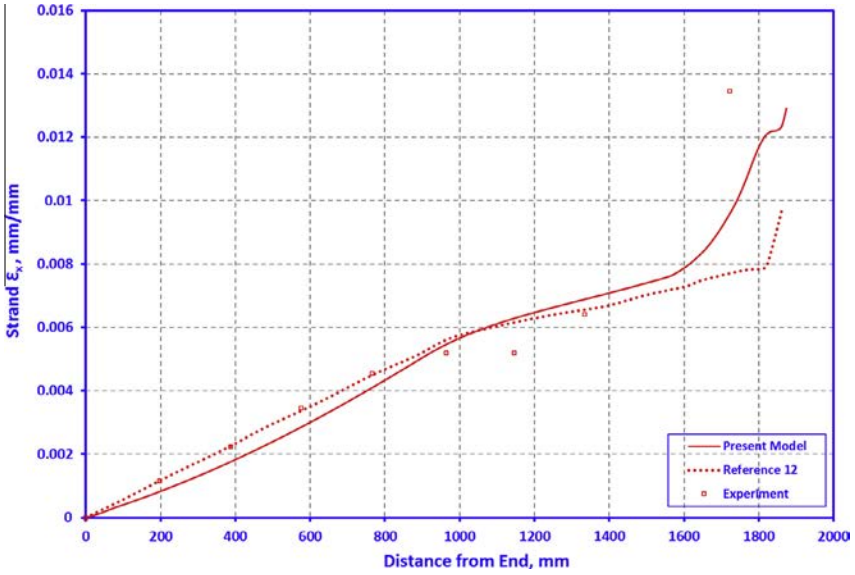

Fig. 21. Variation of limit state strand strain vs. distance from end for problem of Ref. [15].

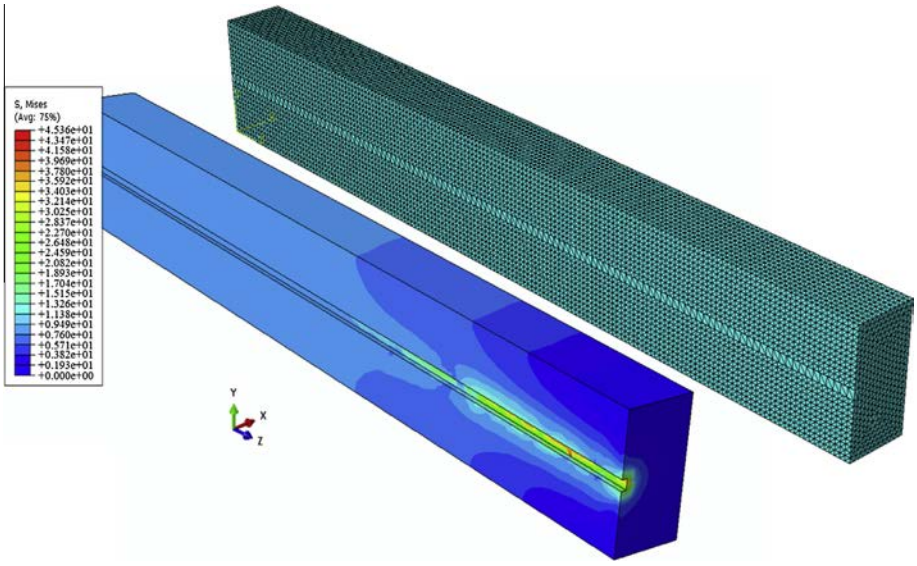

Fig. 22. FE Model (1/4th) of Ref. [16] problem and equivalent stress fringes after transfer (MPa).

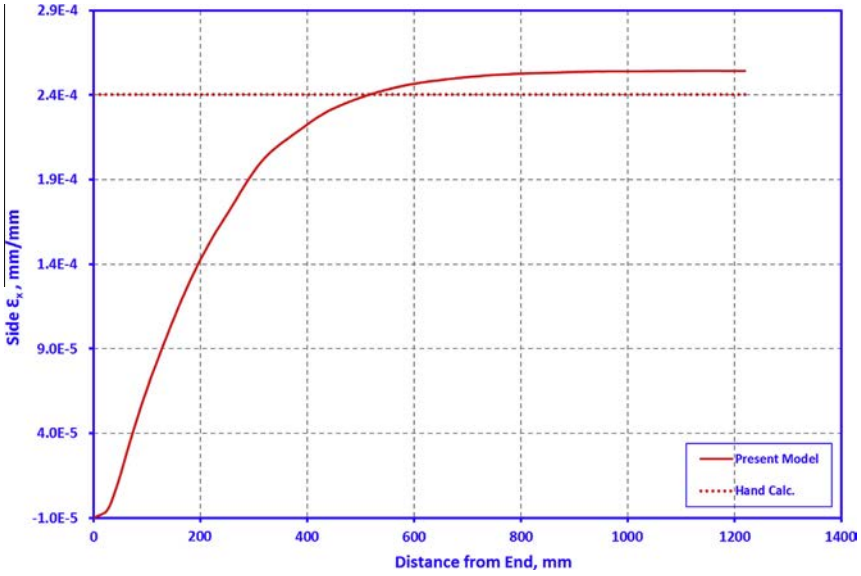

Fig. 23. Variation of side strain vs. distance from end for problem of Ref. [16].

strain is positive. In Fig. 18(a), the location of cracks in the bottom flange, observed during the test before repair, are highlighted by yellow lines. The predicted crack locations in Fig. 18(b) show good agreement with test.

By observing both finite element simulation predictions and the experimental data, it can be concluded that the Carbodur plate spanning the flexure cracks in the bottom flange both arrested the growth of the existing cracks and prevented the formation of new cracks. The local composite patch repair scheme seemed to do its job well.

5. Simulation of problems of references 15, 16 and 17

For further evaluation of the analysis scheme, the problems presented in references 15, 16 and 17 were simulated again with the finite element model proposed by the authors. By comparing the performance of the present model and the models presented in these references, it can easily be concluded that the finite element models of references 15, 16 and 17 are relatively crude and yield inaccurate results. The proposed scheme shows excellent agreement with relevant experimental data of these three problems proving that the presented modeling scheme can properly capture the real behavior of a wide variety of prestressed concrete structures.

5.1. Problem of reference 15

After defining all the material and bond properties appropriately, a finite element model of the problem of reference 15 is created by using the proposed modeling scheme. The results of the model are then compared with the experimental work of Mitchell [35]. All the material and geometric properties of the prestressed concrete beam problem are taken from the associated publications [15,35]. The general mesh configuration and effective

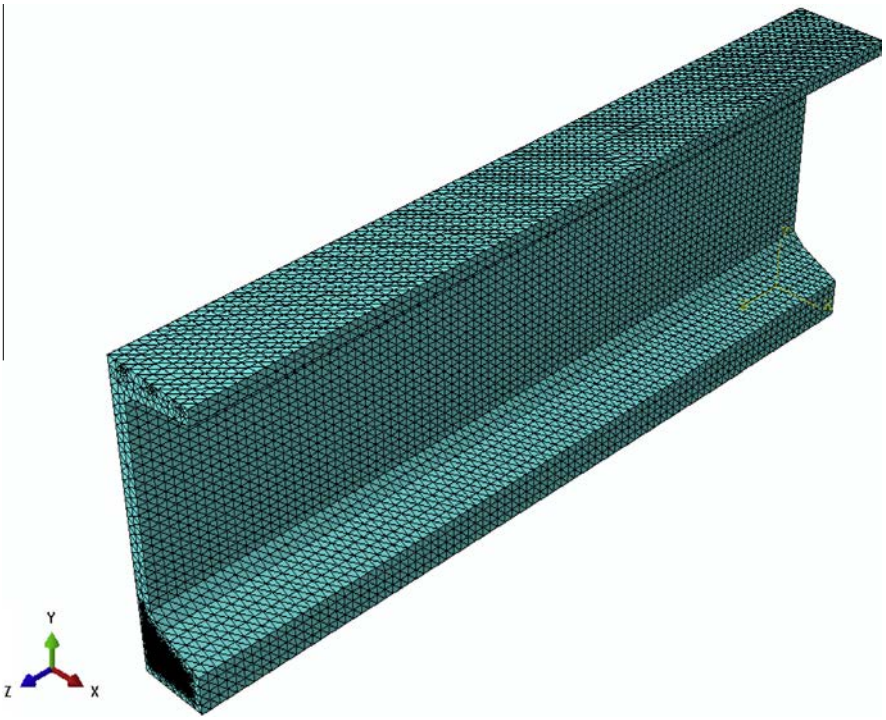

Fig. 24. FE Model (1/4th) of problem of Ref. [17].

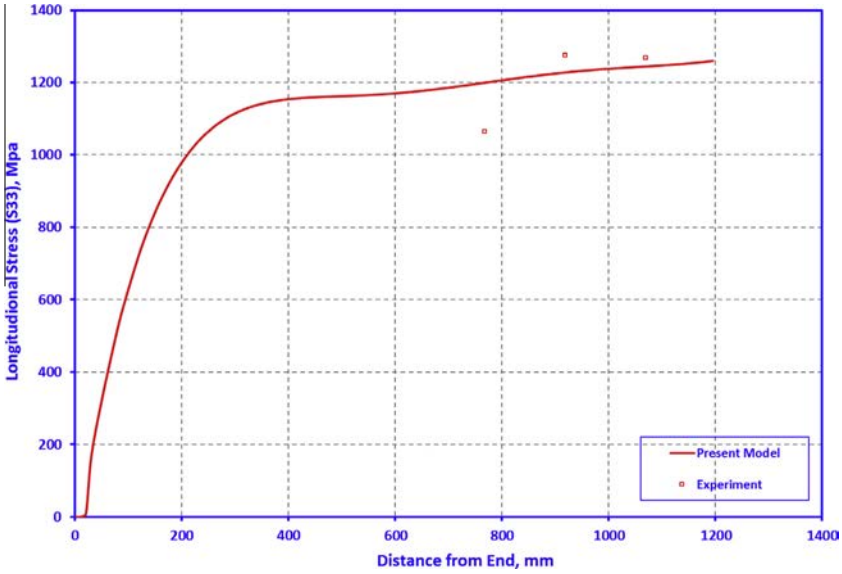

Fig. 25. Variation of longitudinal stress (S33) of the strand "R8C7" vs. distance from end for the problem of Ref. [17].

stress fringes of the finite element model of the beam are shown in Figs. 19 and 20. As can be seen in Fig. 19, all components of the problem is represented in the 3-D domain. The model of reference 15 however, represented the tendons for the same problem in 1-D, which can at best be a gross approximation of the real life behavior. Also, the effects of cracking and tension stiffening in concrete were not properly represented.

In the present analysis, the finite element model of the problem of Ref. [15] reached its limit state at the maximum moment of 46.5 kN m, which is close to the Ref. [35] value. As can be seen in Fig. 21, the proposed finite element model follows the experimental data more closely over the whole length of the beam. It is evident that, the accuracy of the numerical results presented in Ref. [15] is significantly less at locations close to the middle of the beam and closer to the support. Additionally, important data like crack locations of the beam cannot be extracted by the model of Ref. [15]. Locations of the cracks are estimated by comparing the calculated strain values in the concrete with the assumed cracking strain of Ref. [15]. On the other hand, the proposed finite element model gives accurate prediction of crack locations of the beam. The hyperbolic shape of stress contour after the release of strands, which is evident from Fig. 20, verifies the true mechanics of stress transfer is accounted for in the present analysis. This aspect was further checked by undertaking separate runs with strand sections

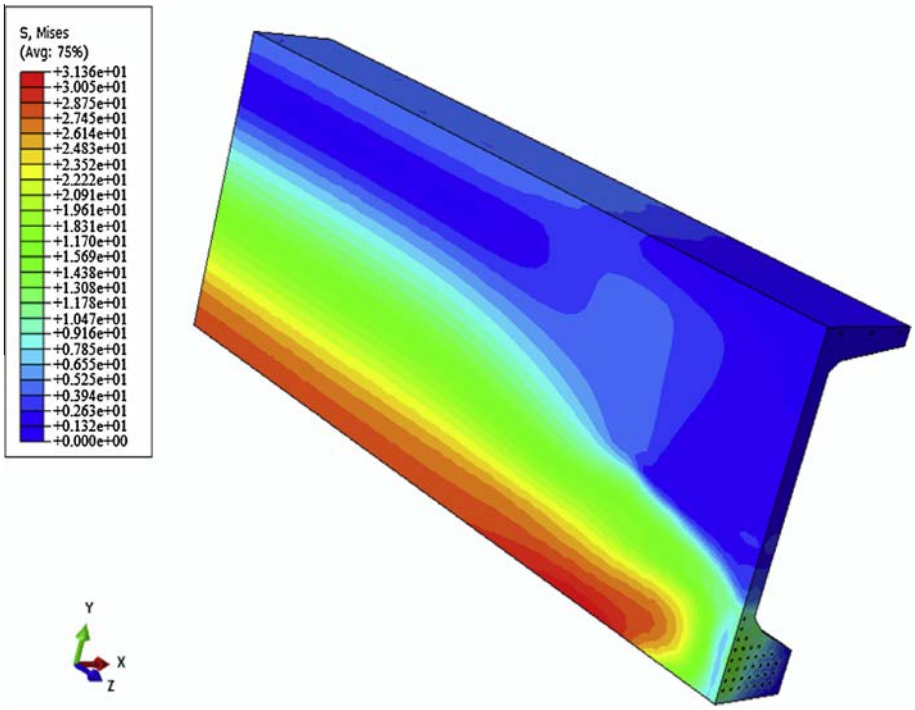

Fig. 26. Equivalent stress fringes after transfer for problem of Ref. [17] (MPa).

modeled as equivalent square and as also as circular and no difference in the results was noticed except that former model required somewhat less computational effort.

5.2. Problem of reference 16

After appropriately defining the material and bond properties, the proposed modeling scheme is applied to the test problem and the results are compared with the experimental data of Akhnoukh [20]. In Ref. [16] and Akhnoukh's [20] studies, results are presented for different stirrup configurations. As negligible difference in the preliminary results of the present simulation was noted for cases with and without stirrup, for computational efficiency, the stirrups were taken out of the subsequent simulations. The finite element model used (on right) and the equivalent stress fringes (on left) are shown in Fig. 22.

As stated before, Ref. [16] results are qualitative and hence could not be compared with. On the other hand, the experimental data used in the associated Ref. [20] was found to be almost two orders of magnitude larger than what was obtained by the present model and further verified by simple hand calculations. Plots of variation of side strain of the beam with respect to the beam length along with the hand calculated value are presented in Fig. 23. Hence, the results from these references could not be relied upon.

5.3. Problem of reference 17

After a similar treatment of the problem of Ref. [17] as in the other two cases, the prestressed concrete finite element model of the problem presented in Ref. [17] is built and simulated and the results are compared with the experimental work of O'Callaghan [21]. As before, since modeling of stirrups did not make any difference in the results, the stirrups have been disregarded during the present modeling process. All the associated material and geometric information for the prestressed concrete beam problem were taken from [17,21]. A view of the finite element model can be seen

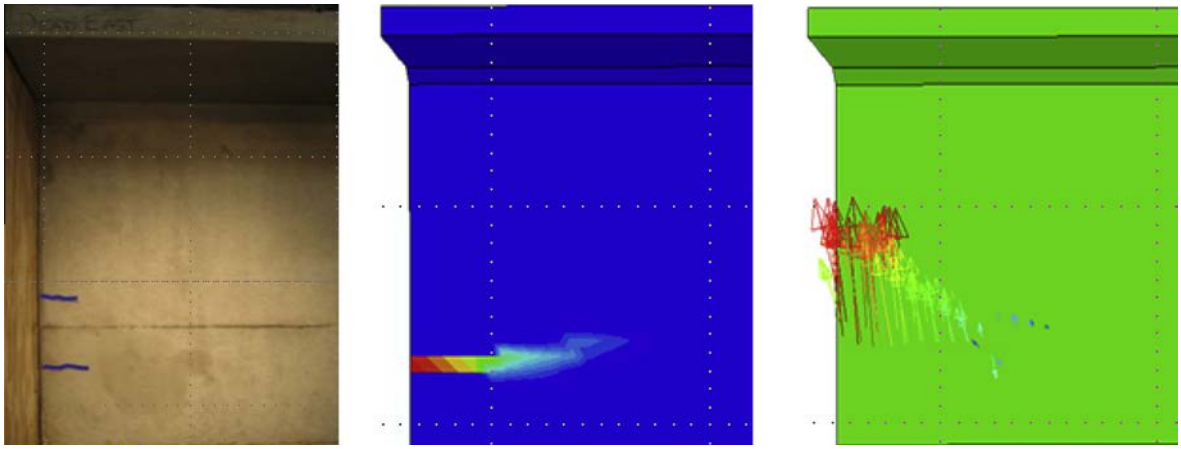

Fig. 27. Experimental cracks at transfer, plots of principal plastic strain fringes, and principal plastic tensile strain directions based on the present model for problem of Ref. [17].

in Fig. 24. As there was no bond property information or test data available corresponding to the strand-concrete bond in the study of O'Callaghan [21], the model of this problem was created with bond properties calculated indirectly on the basis of concrete strength. The comparison of strain values of one of the strands obtained from the present finite element model and the experimental work of O'Callaghan is shown in Fig. 25.

Since prestressing strands are not physically present in the model of Ref. [17], the data shown in Fig. 25 could not be obtained from Okumus's model. As a result, the strand stress values obtained from the present finite element model only have been compared with O'Callaghan's [21] experimental data. Incidentally, in Ref. [17], the only data that has been compared with O'Callaghan's [21] experimental work is the stresses in the stirrups.

Fig. 26 shows the equivalent stress fringes of the present model for Ref. [17] problem after the release of the strands. The hyperbolic variation of equivalent stress around the strands shows that the mechanics of the force transfer between the strands and the concrete is accurately represented in the present model. In Fig. 27 along with the maximum principal plastic strain plot, principal plastic tensile strain directions of the present model with cracks formed after the release of the strands during the experimental work of problem of Ref. [17] is presented. As can be seen from Fig. 27, there is good agreement between the actual behavior of the beam and the present finite element model. On the other hand, in Ref. [17], only the principal strain directions of the total strain are plotted. As far as the cracks in the concrete is concerned, total strain does not help with the identification of the crack formation. As a result, in this study, the principal tensile strain directions of the plastic strain are presented.

6. Conclusions

This paper deals with the realistic finite element simulation of the behavior of pretensioned prestressed concrete beams. The plasticity–damage model for concrete and bond-slip model for steel–concrete interface are discussed. The modeling process faithfully reflected all the loading conditions beginning with strand tensioning operation, stress transfer, and subsequent loading till failure. All the modeling issues were carefully dissected as also the shortcomings of the relatively recent finite element models presented in the current literature were critically evaluated. The data for test beam were obtained from the experimental studies carefully undertaken as part of this effort. The modeling and simulation results for the test problem showed good agreement with test results up to the collapse load. The simulation results gave a clear understanding of the true behavior of such beams. The proposed scheme when implemented with software like Abaqus can be applied both in research and practice. This paper can be considered to have successfully achieved the following objectives:

- Developed an accurate finite element modeling scheme for pretensioned beams based on a plasticity damage and bond-slip failure model.
- Successfully predicted the true behavior of pretensioned concrete beams during the whole history of construction and subsequent external loading.
- Successfully verified the simulation results with two stages of experimental investigation – before and after bonded composite patch strengthening.

A possible improvement to the model may be the explicit inclusion of creep and shrinkage effects in the model to predict the long-term performance.

Acknowledgement

The work presented in this paper was partly supported by a research contract awarded by the Tennessee Department of Transportation.

References

[1] Dhonde H, Mo Y, Hsu T. Fiber reinforcement in prestressed concrete beams. College Station (TX): University of Houston; 2006.
[2] Magnel G. Prestressed concrete. New York (NY): McGraw-Hill; 1954.
[3] Guyon Y. Prestressed concrete. New York (NY): Contractors Record; 1953.
[4] Som P, Ghosh K. Anchor zone stresses in prestressed concrete beams. ASCE J. Struct. Div. 1964;90:49–62.
[5] Iyengar K, Prabhakara M. Anchor zone stresses in prestressed concrete beam. ASCE J Struct Div 1971;97:807–24.
[6] Iyengar K. Two dimensional theories of anchorage zone stresses in post-tensioned prestressed beams. J Am Concr Inst (ACI) 1962;59(10):1443–65.
[7] Marshall W, Mattock A. Control of horizontal cracking in the ends of pretensioned prestressed concrete girders. Prestr Concr Inst (PCI) J 1962;7(5):56–74.
[8] Gergely P, Sozen M. Design of anchorage-zone reinforcement in prestressed concrete beams. Prestr Concr Inst (PCI) J 1967;12(2):63–75.
[9] Padmarajaiah S, Ramaswamy A. A finite element assessment of flexural strength of prestressed concrete. Cement Concr Compos 2002;24(2):229–41.
[10] Markovic M, Kraberger N, Saje M, Planinc I, Bratina S. Non-linear analysis of pre-tensioned concrete planar beams. Eng Struct 2013;46:279–93.
[11] Lou T, Xiang Y. Finite element modeling of concrete beams prestressed with external tendons. Eng Struct 2006;28:1919–26.
[12] Building Code Requirements for Structural Concrete and Commentary (ACI 318M-11). American Concrete Institute (ACI); 2011.
[13] AASHTO LRFD Bridge Design Specifications. American Association of State Highway and Transportation Officials (AASHTO); 2010.
[14] Tuchscherer R, Birrcher D, Bayrak O. Strut-and-tie model design provision. Prestr Concr Inst (PCI) J 2011;56(1):155–70.
[15] Ayoub A, Filippou F. Finite-element model for pretensioned prestressed concrete girders. ASCE J Struct Eng 2010;136(4):401–9.
[16] Arab A, Badie S, Manzari M. A methodological approach for finite element modeling of pretensioned concrete members at the release of pretensioning. Eng Struct 2011;33(6):1918–29.
[17] Okumus P, Oliva M, Becker S. Nonlinear finite element modeling of cracking at ends of pretensioned bridge girders. Eng Struct 2012;40:267–75.
[18] Taylor R. FEAP finite element analysis program user manual. Berkeley (CA): University of California at Berkeley; 2005.
[19] Abaqus. Analysis user's guide v6.13. Providence (RI): Dassault Systèmes; 2013.
[20] Akhnoukh A. Development of high performance precast/prestressed bridge girders. Lincoln (NE): University of Nebraska-Lincoln; 2008.
[21] O'Callaghan M, Bayrak O. Tensile stresses in the end regions of pretensioned I-beams at release. Austin (TX): Texas Department of Transportation; 2008.
[22] Lee J, Fenves G. Plastic-damage model for cyclic loading of concrete structure. J Eng Mech 1998;124(8):892–900.
[23] Lubliner J, Oliver J, Oller S, Onate E. A plastic-damage model for concrete. Int J Solids Struct 1989;25(3):299–326.
[24] Kachanov L. Introduction to continuum damage mechanics. Brookline (MA): Martinus Nijhoff Publishers; 1986.
[25] Hognestad E, Hanson NW, McHenry D. Concrete stress distribution in ultimate strength design. Am Concr Inst (ACI) J Proc 1955;52(12):455–80.
[26] Akita H, Koide H, Tomon M, Sohn D. A practical method for uniaxial tension test of concrete. Mater Struct 2003;36(6):365–71.
[27] Carpinteri A, Invernizzi S. Influence of damage on the fractal properties of concrete subjected to pure tension. Mater Struct 2001;34(10):605–11.
[28] van Vliet M. Size effect of tensile fracture in concrete and rock. Delft, Netherlands: Delft University of Technology; 2000.
[29] PCI design handbook precast and prestressed concrete. Chicago, IL: Prestressed Concrete Institute (PCI); 2004.
[30] Cheok G, Stone W. Performance of 1/3 scale model precast concrete beam-column connections subjected to cyclic inelastic loads. Gaithersburg (MD): NISTIR; 1994.
[31] Yeih W, Huang R, Chang J, Yang C. A pull-out test for determining interface properties between rebar and concrete. Adv Cem Based Mater 1997;5(2):57–65.
[32] Yapar O, Basu P, Seger W, McNutt J, Nordendale N. Local repair of precast concrete beams using bonded composite patch. In: PCI national bridge conference. Nashville (TN); 2012.
[33] Yapar O. AE based health monitoring and bonded FRP patch repair in bridge management. Nashville, TN: Dissertation. Vanderbilt University; 2015.
[34] Libby J. Modern prestressed concrete. New York (NY): Van Nostrand Reinhold; 1977.
[35] Mitchell D, Cook W, Khan AA, Tham T. Influence of high strength concrete on transfer and development length of pretensioning strand. Prestr Concr Inst (PCI) J 1993;38(3):52–66.